Heating Structures of the TRMM Field Campaigns

COURTNEY SCHUMACHER

Department of Atmospheric Sciences, Texas A&M University, College Station, Texas

MINGHUA H. ZHANG

Institute for Terrestrial and Planetary Atmospheres, Marine Sciences Research Center, Stony Brook University, Stony Brook, New York

PAUL E. CIESIELSKI

Department of Atmospheric Science, Colorado State University, Fort Collins, Colorado

(Manuscript received 25 January 2006, in final form 31 August 2006)

ABSTRACT

Heating profiles calculated from sounding networks and other observations during three Tropical Rainfall Measuring Mission (TRMM) field campaigns [the Kwajalein Experiment (KWAJEX), TRMM Large-Scale Biosphere–Atmosphere Experiment in Amazonia (LBA), and South China Sea Monsoon Experiment (SCSMEX)] show distinct geographical differences between oceanic, continental, and monsoon regimes. Differing cloud types (both precipitating and nonprecipitating) play an important role in determining the total diabatic heating profile. Variations in the vertical structure of the apparent heat source, Q_1, can be related to the diurnal cycle, large-scale forcings such as atmospheric waves, and rain thresholds at each location. For example, TRMM-LBA, which occurred in the Brazilian Amazon, had mostly deep convection during the day while KWAJEX, which occurred in the western portion of the Pacific intertropical convergence zone, had more shallow and moderately deep daytime convection. Therefore, the afternoon height of maximum heating was more bottom heavy (i.e., heating below 600 hPa) during KWAJEX compared to TRMM-LBA. More organized convective systems with extensive stratiform rain areas and upper-level cloud decks tended to occur in the early and late morning hours during TRMM-LBA and KWAJEX, respectively, thereby causing Q_1 profiles to be top heavy (i.e., maxima from 600 to 400 hPa) at those times. SCSMEX, which occurred in the South China Sea during the monsoon season, had top-heavy daytime and nighttime heating profiles suggesting that mesoscale convective systems occurred throughout the diurnal cycle, although more precipitation and upper-level cloud in the afternoon caused the daytime heating maximum to be larger. A tendency toward bottom- and top-heavy heating profile variations is also associated with the different cloud types that occurred before and after the passage of easterly wave troughs during KWAJEX, the easterly and westerly regimes during TRMM-LBA, and the monsoon onset and postonset active periods during SCSMEX. Rain thresholds based on heavy, moderate, and light/no-rain amounts can further differentiate top-heavy heating, bottom-heavy heating, and tropospheric cooling. These budget studies suggest that model calculations and satellite retrievals of Q_1 must account for a large number of factors in order to accurately determine the vertical structure of diabatic heating associated with tropical cloud systems.

1. Introduction

The apparent heat source, Q_1, is the heating that results from unresolved diabatic processes in the atmosphere, for example, cloud systems within a sounding network that spans a region on the order of 10 000 km^2. Yanai et al. (1973) popularized the term as a way to relate large-scale motion and organized cumulus convection. The ability to characterize variations in Q_1, especially its vertical structure, allows greater understanding of the relationship between tropical convective cloud systems and the large-scale circulation (e.g., Hartmann et al. 1984).

Corresponding author address: Courtney Schumacher, Department of Atmospheric Sciences, Texas A&M University, 3150 TAMU, College Station, TX 77843-3150.
E-mail: courtney@ariel.met.tamu.edu

DOI: 10.1175/JAS3938.1

Here it is shown that Q_1 can be defined as follows:

$$Q_1 = \frac{\partial \overline{s}}{\partial t} + \overline{\nabla \cdot (s\mathbf{V})} + \frac{\partial(\overline{s}\,\overline{\omega})}{\partial p} \quad (1)$$

$$= Q_R + L(c - e) - \frac{\partial(\overline{s'\omega'})}{\partial p}, \quad (2)$$

where s is the dry static energy, $s = c_p T + gz$ (i.e., the sum of enthalpy and potential energy), Q_R is the atmospheric radiative heating or cooling, $L(c - e)$ is the latent heating or cooling resulting from phase changes of water (here indicated by the latent heat of vaporization times condensation minus evaporation, but more generally including the latent heat of fusion times freezing minus melting and the latent heat of sublimation times deposition minus sublimation), and $\overline{s'\omega'}$ is the vertical eddy transport of sensible heat. Overbars represent the average over the budget area; primes represent subgrid-scale deviations from the area average.

Equation (1) determines Q_1 as the residual of sounding network measurements of wind and temperature (Reed and Recker 1971; Yanai et al. 1973; Johnson 1976; Thompson et al. 1979). Similar calculations can be made with gridded model output (e.g., Nigam et al. 2000) or reanalysis fields (e.g., Sardeshmukh 1993); however, this study will focus on Q_1 estimates from sounding budgets. Equation (2) determines Q_1 using direct observations of the cloud systems, such as precipitation and cloud extent, to estimate the radiative, latent, and sensible heating components (Houze 1982, 1989). Separate observations are normally required to determine each term, or alternatively, cloud-resolving models can be used (Tao et al. 1990). During precipitation events, latent heating is generally the largest component of Q_1, followed by radiative heating and the convergence of vertical eddy heat flux.

Based on the earlier sounding budget studies listed above, distinct geographical variations in the vertical structure of Q_1 have been found. For example, Reed and Recker (1971) showed that the peak in Q_1 occurs near 400 hPa (or ~7 km) over the tropical west Pacific, while Thompson et al. (1979) indicated a more bottom-heavy profile over the tropical east Atlantic with a maximum in Q_1 at 600 hPa (or ~4 km). These geographical variations in the height of the Q_1 peak have significant implications for the large-scale circulation (Schumacher et al. 2004).

The Q_1 profiles also exhibit large temporal variations based on the existence and evolution of cloud systems within the sounding network (e.g., Fig. 10 of Lin and Johnson 1996). Time periods with little or no convection show negative Q_1 values throughout the depth of the troposphere, essentially representing clear-sky radiative cooling. Positive Q_1 values indicate the presence of clouds and precipitation; the relative occurrence of each cloud type and how much the clouds precipitate largely determine the vertical structure of the Q_1 profile. Figure 1 illustrates idealized latent heating profiles (the largest component of Q_1) for different types of convection. The basis of the profiles is further described in Schumacher et al. (2004). Note that the magnitude of the precipitating cloud profiles is arbitrary until a precipitation amount is assigned. Shallow convective cells (in this paper meant to encompass a broad height range of precipitating cells with cloud tops generally not exceeding 400–500 hPa) have a heating maximum in the lower troposphere (~800 hPa), deep convective cells have a heating maximum in the midtroposphere (~600 hPa), and stratiform rain areas have a heating maximum in the mid-to-upper troposphere (~400 hPa) and cooling in the lower troposphere. In situations with low- or midlevel stability (such as commonly observed at the trade inversion or 0°C level; see Johnson et al. 1999) or dry air aloft, cumulus clouds heat the lower levels of the atmosphere, but cool the mid- and upper levels where cloud water and ice particles are detrained. The shape and magnitude of this profile is dependent on the height of the cumulus clouds and the amount of cloud material detrained. The solid line in Fig. 1 illustrates an idealized profile for strongly detraining cumulus congestus clouds (cf. the 28 June Q_1 profile in Nitta and Esbensen 1974). The rather broad cooling between 400 and 600 mb is meant to encompass a range of detrainment heights; that is, the idealized profile is supposed to represent an aggregate of strongly detraining cumulus clouds.

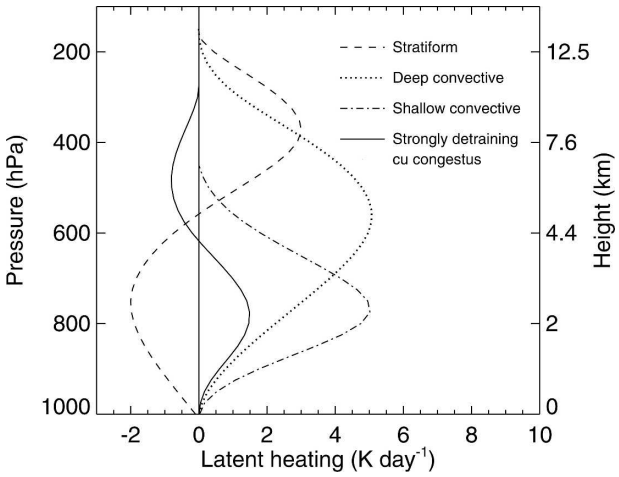

FIG. 1. Idealized latent heating profiles for different precipitating cloud types.

A main objective of the National Aeronautics and

Space Administration's (NASA) Tropical Rainfall Measuring Mission (TRMM) was to use satellite and ground observations of tropical rain systems to derive the four-dimensional distribution of heating to better understand global climate (Simpson et al. 1988). Toward this end, three field programs were carried out in very different climatological regimes (oceanic, continental, and monsoonal) in order to validate and improve the physical assumptions used in TRMM satellite retrievals: the Kwajalein Experiment (KWAJEX), the TRMM Large-Scale Biosphere–Atmosphere Experiment in Amazonia (TRMM-LBA), and the South China Sea Monsoon Experiment (SCSMEX). There are inherent limitations in using relatively short field campaign datasets to describe the climatology of a region. With that awareness, this paper uses observations from each of these campaigns to characterize variations in Q_1 associated with convective systems observed in the Tropics.

2. The TRMM field campaigns

a. KWAJEX

KWAJEX occurred in the Marshall Islands (7°–10°N, 166°–169°E; Fig. 2a) from 24 July to 15 September 1999 with the purpose of studying convective processes over the open tropical ocean and how these processes relate to TRMM satellite retrievals (Yuter et al. 2005). The Kwajalein atoll is composed of very small islands with negligible land surface such that the diurnal cycle of rainfall is weak (Schumacher and Houze 2000) and atmospheric waves appear to play a more important role in convective organization (Sobel et al. 2004; Cetrone and Houze 2006). Thus, synoptic-scale forcing would be assumed to cause the most distinct domain-averaged temporal variations in Q_1 profiles over Kwajalein.

b. TRMM-LBA

TRMM-LBA occurred in the southwestern Brazilian Amazon (13°–9°S, 64°–60°W; Fig. 2b) in January and February 1999 and was organized to observe convective processes over a tropical continent and how these processes relate to TRMM satellite retrievals (Silva Dias et al. 2002). We will focus on the more intensive observation period from 24 January to 28 February. Many of the published results from TRMM-LBA stress differences in convective systems between the easterly and westerly low-level wind regimes as measured in the southwest Amazon (Halverson et al. 2002; Laurent et al. 2002; Rickenbach et al. 2002). During the easterly regime, convective systems had more intense convection and higher ice-scattering signatures and produced

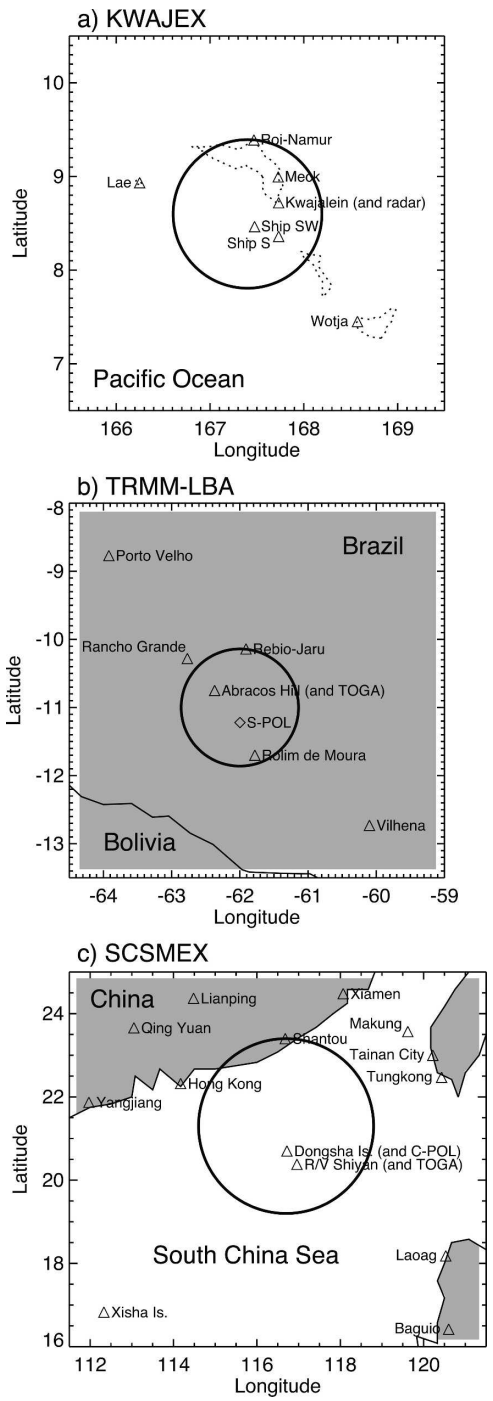

FIG. 2. (a)–(c) The variational analysis domains (thick circles) for each field campaign. Note that each plot has different dimensions. Sounding sites are indicated by triangles and radars are indicated by a diamond or are shown in parentheses. The dotted lines in (a) indicate the outlines of atolls (i.e., coral islands enclosing a lagoon); the rest of the region is open ocean. The shading in (b),(c) represents land areas.

more lightning. During the westerly regime, convective cells were weaker and relatively more stratiform rain was produced, ice-scattering signatures decreased, and lightning occurred less frequently. These regime-based variations in convective system characteristics were also shown to occur in multiple years of wet-season TRMM satellite observations (Petersen et al. 2002). Diurnal variations in convective systems during TRMM-LBA have also been studied (Betts et al. 2002; Machado et al. 2002; Cifelli et al. 2004; Rickenbach 2004; Strong et al. 2005). The diurnal maxima in rainfall and rain area occurred in the afternoon, while secondary maxima occurred in the early morning hours. The diurnal cycle in the boundary layer was also shown to be weaker during the westerly regime. All of these factors affect the resultant Q_1 fields.

c. *SCSMEX*

SCSMEX occurred in the South China Sea from 1 May–30 June 1998 in order to study the onset and evolution of the Southeast Asian monsoon (Lau et al. 2000). Two intensive observing networks were established during SCSMEX: one over the northern South China Sea and another over the southern South China Sea (Ciesielski and Johnson 2006). This study will focus on the northern oceanic network (19°–24°N, 114°–119°E; Fig. 2c) where data coverage (sondes and radar) was better and on the period from 6 May to 20 June when sonde coverage over the domain was most complete. The 30–60-day oscillation, modified by a 10–20-day mode, played a large role in the active and break periods of the 1998 monsoon (Chan et al. 2002). During the different phases of the monsoon, a large variety of storm systems and convective structures were observed (Lau et al. 2002; Johnson and Ciesielski 2002; Wang 2004; Johnson et al. 2005). Convective systems during the onset and break periods were relatively weak with a small fraction of stratiform rain. Convective systems during the postonset active phase were more organized with higher stratiform rain fractions. These variations have large implications for the Q_1 vertical structure (Johnson and Ciesielski 2002; Tao et al. 2003).

3. Variational analysis

The variational analysis approach of Zhang and Lin (1997) is used to derive the Q_1 profiles in this study. Because of instrument and measurement uncertainties and scale aliasing in the radiosonde data, budget analyses from sounding networks often suffer from large errors (Ooyama 1987; Mapes et al. 2003a). The variational approach constrains the sounding data to satisfy column-integrated budgets of mass, energy, and moisture. This process adjusts the atmospheric winds, temperature, and humidity by the minimum possible amount. Zhang and Lin (1997) showed that the magnitudes of the adjustments are typically smaller than instrument and measurement uncertainties, yet they may have a large impact on the derivative fields. The variational analysis requires the use of error variances of the control variables. These error variances are specified as in Zhang et al. (2001).

Uncertainties in the analyzed Q_1 are from several sources: measurements of surface energy and water fluxes as constraints, specification of error variances in the atmospheric state variables, and errors associated with the calculation of the horizontal transport terms. Since the vertically integrated heating is constrained by surface measurements, the uncertainty of the overall magnitude of the heating profiles should be similar to that of the constraining variables. The vertical structure of the heating profiles is somewhat dependent on the specified error variances, but the impact is expected to be secondary in nature. Previous sensitivity studies suggest that the largest uncertainty of the analyzed heating is from surface precipitation as a constraint (Zhang et al. 2001). Because errors in surface measurements averaged over a small domain are typically larger than those averaged over a large domain, we expect the uncertainties of the heating profiles to differ between the three experiments. Therefore, the percentage uncertainties of the heating profiles can be assumed as similar to those of the domain-averaged precipitation in the respective field experiments. In addition, the present paper uses composites of Q_1 from the variational analysis, which will reduce uncertainties due to sampling errors (Mapes et al. 2003a).

The following paragraph details the constraint datasets used in the variational analysis.

Radiative fluxes at the surface and top of the atmosphere (TOA) for the energy constraint were obtained from the International Satellite Cloud Climatology Project (ISCCP; Rossow et al. 1996). ISCCP data are at 2.5° resolution, so an average over the nearest grid points to the variational analysis domains was used. For the surface net radiative flux at TRMM-LBA, the ISCCP values were adjusted to the tower measurements from the University of Virginia. Area-averaged latent and sensible heat fluxes were based on reanalysis values adjusted to surface station measurements. KWAJEX and TRMM-LBA area-averaged latent and sensible heat fluxes were from the National Centers for Environmental Prediction (NCEP) reanalysis adjusted to flux measurements made by the University of Virginia at Meck Island and Ji Parana, Brazil, respectively.

SCSMEX fluxes were from the Japanese Meteorological Agency (JMA) reanalysis adjusted to flux measurements made on the R/V *Shiyan #3*. Rain measurements from rain gauges, radar, and satellites were used when available. KWAJEX rainfall was based on ground radar precipitation maps from the University of Washington (Houze et al. 2004) and TRMM-LBA rainfall was based on hourly averaged radar precipitation maps, which agree well with data from the surface rain gauge networks (Carey et al. 2000). SCSMEX rainfall was based on 3-h TRMM 3B42 Version 6 precipitation estimates and gauge data at Dongsha Island.

The configurations of the sounding networks were not ideal for carrying out traditional budget studies due to logistical difficulties in the TRMM field campaigns, particularly for the KWAJEX and TRMM-LBA networks (Figs. 2a,b). Zhang et al. (2001) proposed to combine the traditional line integral and regular grid methods under these circumstances so that an analysis grid may take sounding measurements from multiple stations, including stations well outside of the variational analysis domain. For example, operational soundings available at 0000 and 1200 UTC from Porto Velho and Vilhena (as well as other operational soundings not pictured) were used to supplement the four TRMM-LBA enhanced sounding sites (Fig. 2b). The NCEP upper analysis was used as a background for KWAJEX and TRMM-LBA and the JMA Global Energy and Water Cycle Experiment (GEWEX) Asian Monsoon Experiment (GAME) V1.1 reanalysis, available at 6-h and 2.5° resolution, was used as the background for SCSMEX. The analysis domains for the three experiments are shown by the thick circles in Fig. 2—all surface and TOA constraint variables were averaged for these areas. Note that the SCSMEX variational analysis domain has a diameter roughly twice the size of the KWAJEX and TRMM-LBA domains. In addition, Roy et al. (2004) found a dry bias in the ship soundings in KWAJEX and two of the sites in TRMM-LBA, which was not accounted for in the following analysis. Variational analysis output has a temporal resolution of 6 h and a vertical resolution of 25 hPa. [Variational analysis input data and output fields for each field campaign are available online at http://www.atmos.washington.edu/gcg/MG/KWAJ/lh.html (KWAJEX), http://tornado.atmos.colostate.edu/lbadata (TRMM-LBA), and http://tornado.atmos.colostate.edu/scsmexdata (SCSMEX).] The total number 6-h samples for each field campaign is: KWAJEX: 210, TRMM-LBA: 142, and SCSMEX: 182.

Figures 3a–c shows the 6-h precipitation time series used as a variational analysis constraint for each field campaign. The average daily rainfall rates within each analysis domain were: KWAJEX: 6.1 mm, TRMM-LBA: 6.6 mm, and SCSMEX: 11.4 mm (Table 1). During KWAJEX (Fig. 3a), convective events were short-lived (or traveled through the budget domain rapidly) and appeared to have a 4–5-day variability, possibly associated with wave activity. The horizontal lines indicate the passage of easterly wave troughs (solid) and ridges (dashed) based on the low-level meridional wind field and are discussed further in section 5. The convective events during TRMM-LBA (Fig. 3b) were also somewhat short-lived but appear to be linked to the diurnal cycle rather than large-scale waves. The easterly and westerly regimes are shown for reference and are also discussed in section 5. The time series for SCSMEX (Fig. 3c) indicates extended active and quiescent periods linked to the evolution of the monsoon. SCSMEX also had a strong diurnal cycle of rainfall. The diurnal cycle of Q_1 at each location is investigated in section 4.

Figures 3d–f show the variational analysis Q_1 time series for each field campaign. During KWAJEX (Fig. 3d), convective events that have strong heating through much of the troposphere are associated with the largest rainfall peaks in Fig. 3a. In addition, the signature of heating at low levels and cooling at mid to upper levels is common. Rangno and Hobbs (2005) directly observed several strongly detraining cumulus congestus clouds from the University of Washington Convair-580 research aircraft in a 15-day period during KWAJEX, so this signature may be associated with cumulus growth at low levels and evaporation of cloud material aloft. The average KWAJEX divergence profile (not shown) indicates strong divergence at 500 hPa, which supports the existence of midlevel detrainment. In addition, radiative cooling could be a significant contributor to the cooling signature aloft. Large Q_1 heating during TRMM-LBA (Fig. 3e) is also linked to large rainfall peaks in Fig. 3b and the profile of heating at upper levels and cooling at lower levels associated with stratiform rain areas is prevalent. This feature of the time series will be further discussed in the next section. The Q_1 time series for SCSMEX (Fig. 3f) shows strong, elevated heating during much of the onset and postonset active monsoon periods and is in good agreement with a separate sounding budget analysis performed by Johnson and Ciesielski (2002). Figure 3 indicates that the three TRMM field campaigns represent a wide range of environments that can affect convective organization and the resultant vertical heating structure.

Figure 4 compares the average Q_1 profiles of each field campaign. While KWAJEX and TRMM-LBA had similar total rain amounts, the average vertical struc-

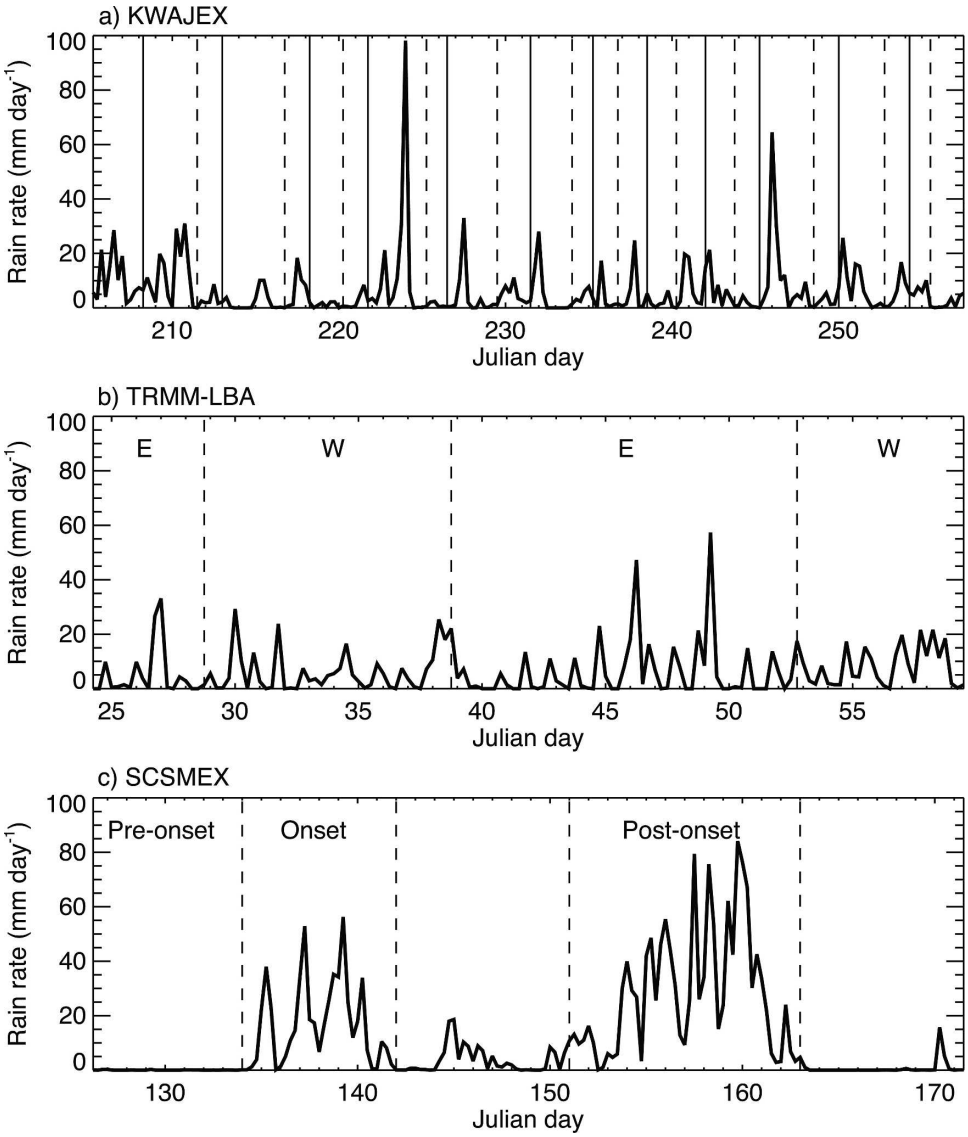

FIG. 3. The precipitation time series based on 6-h data for (a) KWAJEX: solid and dashed lines represent easterly wave trough and ridge passages, respectively, (b) TRMM-LBA: E and W represent the easterly and westerly low-level wind regimes, and (c) SCSMEX: preonset, onset, and postonset represent phases of the Southeast Asian monsoon. (d)–(f) Q_1 variational analysis time series for (a)–(c).

ture and magnitude of Q_1 are very different. In particular, column-integrated Q_1 for KWAJEX and TRMM-LBA is 0.9 and 1.9 K day^{-1}, respectively. Vertically integrating (2) yields $\langle Q_1 - Q_R \rangle = P_0 + \text{SH}$, where $\langle\ \rangle$ denotes the vertical integral, P_0 is surface rainfall, and SH is the surface sensible heat flux, which in rainy regimes is typically much smaller than the other terms. Table 1 shows that $\langle Q_R \rangle$ for KWAJEX is -0.9 K day^{-1} versus -0.2 K day^{-1} for TRMM-LBA such that $\langle Q_1 - Q_R \rangle$ (and thus rainfall) for these two networks is similar. In addition, surface sensible heat fluxes (or SH) were slightly stronger during TRMM-LBA. This exercise reconciles the difference in magnitude between the KWAJEX and TRMM-LBA Q_1 profiles as well as stresses the importance of considering the Q_R component in the overall heating associated with tropical cloud systems.

Figure 4 shows that KWAJEX has two peaks in heating, one near 750 hPa and another at 550 hPa [similar to the height of the peaks observed in the east Atlantic during Global Atmospheric Research Programme (GARP) Atlantic Tropical Experiment (GATE) by

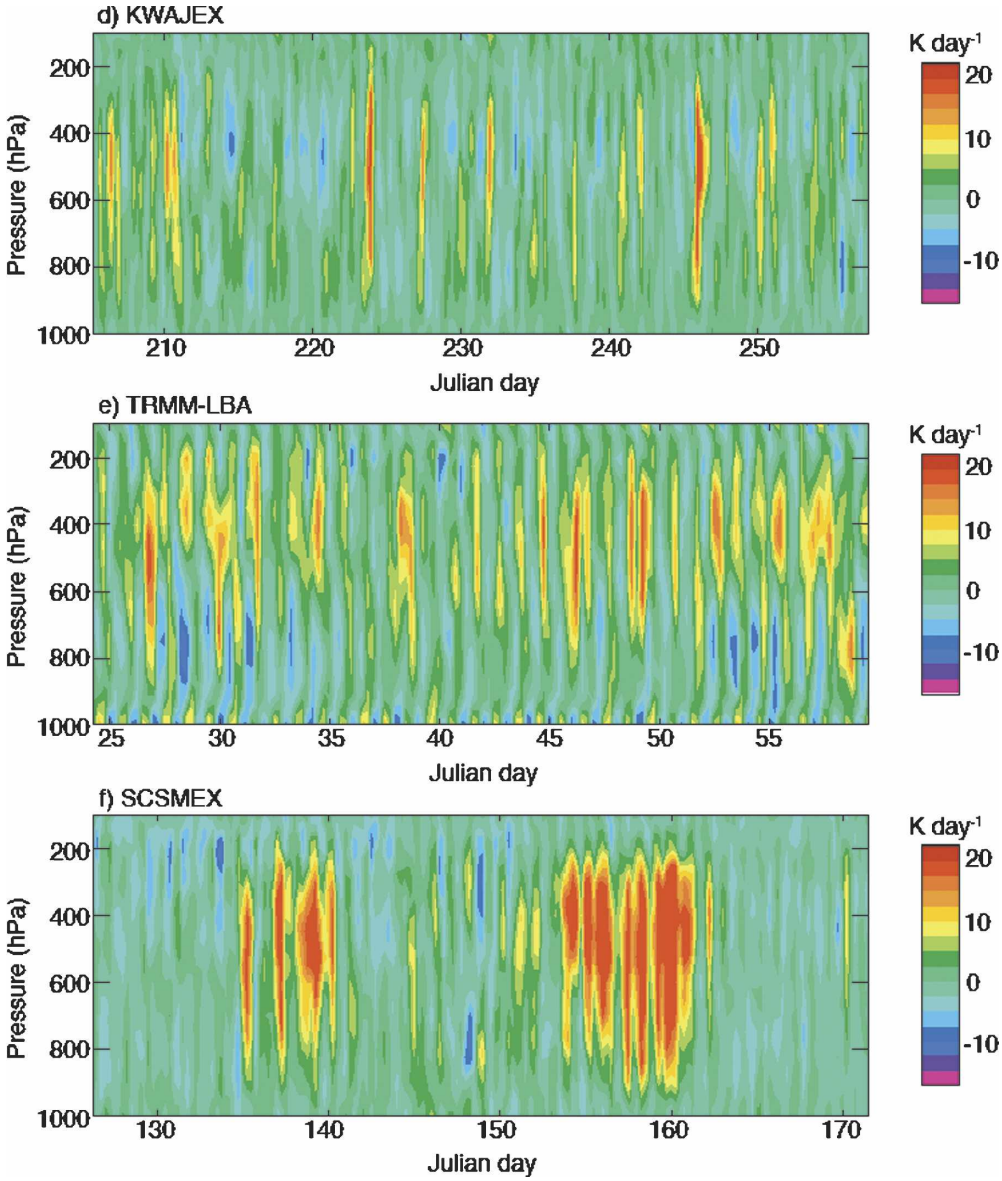

FIG. 3. (*Continued*)

Thompson et al. (1979)]. Both peaks are less than 2 K day^{-1} in magnitude. The low-level peak in the KWAJEX profile likely indicates the prevalence of shallow precipitating convection and the midlevel peak is probably associated with deep convection. TRMM-LBA has an elevated maximum of 5 K day^{-1} near 400 hPa and very little low-level heating, which suggests a large stratiform rain component and a lack of shallow convection. The SCSMEX Q_1 profile has a large elevated heating maximum of 5.4 K day^{-1} at 400 hPa (a similar upper-level peak has been observed in other tropical west Pacific studies, e.g., Lin and Johnson 1996). The large daily rain amounts were likely associated with organized systems composed of large areas of stratiform rain. While there is not a distinct low-level peak in the SCSMEX profile, the existence of moderate low-level heating suggests that shallow convection contributes to the overall heating associated with the monsoon cloud systems. The radar analysis of Johnson et al. (2005) has shown that shallow convective cells were prevalent in SCSMEX during periods of dry conditions aloft and weak instability.

4. Diurnal Q_1 variations

To explore the role the diurnal cycle plays in vertical heating variations, Fig. 5 shows average daytime and

TABLE 1. Diurnal average rain rates and $\langle Q_R \rangle$, where $\langle\rangle$ denotes a column-integrated value.

	KWAJEX			TRMM-LBA			SCSMEX		
UTC	LT	Rain rate (mm day^{-1})	$\langle Q_R \rangle$ (K day^{-1})	LT	Rain rate (mm day^{-1})	$\langle Q_R \rangle$ (K day^{-1})	LT	Rain rate (mm day^{-1})	$\langle Q_R \rangle$ (K day^{-1})
0000	12	7.2	0.3	20	6.6	−1.1	08	11.4	−0.5
0600	18	5.5	−0.8	02	5.8	−1.7	14	14.8	0.4
1200	00	5.4	−1.8	08	2.3	0.6	20	10.2	−1.5
1800	06	6.4	−1.2	14	11.7	1.5	02	8.9	−1.9
Average		6.1	−0.9		6.6	−0.2		11.4	−0.9

nighttime Q_1 profiles along with the total average profile from Fig. 4 for each field campaign. A quarter of all profiles went into each diurnal average (i.e., 52–53 profiles for KWAJEX, 35–36 profiles for TRMM-LBA, and 45–46 profiles for SCSMEX). Typically, 20% or more of a field campaign's 6-h Q_1 profiles were used in the composites analyzed throughout the paper to decrease potential errors from poor sampling. Table 1 shows the diurnal cycle of daily rain rate and $\langle Q_R \rangle$; that is, the column-integrated Q_R.[1] Note that while each campaign had varying diurnal amplitudes in rain rate (and thus column-integrated latent heating), the amplitude of the diurnal cycle of $\langle Q_R \rangle$ in KWAJEX, TRMM-LBA, and SCSMEX was 2.1, 3.2, and 2.3 K day^{-1}, respectively, which represents a significant fraction (~30%) of the diurnal variation seen in the Q_1 profiles in Fig. 5.

Kwajalein is located in the open ocean, which has a weak diurnal cycle of surface temperature. However, the KWAJEX Q_1 profiles show significant diurnal variations (Fig. 5a). The 1200 local time (LT) profile has a maximum of 4 K day^{-1} near 500 hPa likely resulting from of a mix of deep convective and stratiform precipitating systems. Visual observations of clouds made 3 times daily from Kwajalein Island during KWAJEX (cloud photos and synoptic code designations are available online at www.atmos.washington.edu/kwajex/ops-web/cloud_photos) indicate a maximum in cumulonimbus and nimbostratus at this time of day. The upper-level heating maximum is consistent with studies that show more organized systems occur in the early morning over the tropical ocean (e.g., Nesbitt and Zipser 2003), although there is a shift during KWAJEX to late morning. A simple t test shows that this profile is significantly different from the other times above 500 hPa. The 1800 LT profile has a broad maximum of 2.5 K day^{-1} between 800 and 550 hPa, indicative of a range of shallow to deep convection. The 0000 LT profile has a low-level maximum of 1 K day^{-1} at 800 hPa (which is significantly different than the broad heating maximum at 1800 LT by a t test) and an upper-level minimum of −1.5 K day^{-1} at 400 hPa. While this vertical heating structure appears similar to the strongly detraining cumulus congestus latent heating profile in Fig. 1, the degree to which the upper-level cooling is due to detrainment is uncertain. Table 1 shows that radiative cooling is at its maximum at midnight such that if one assumes Q_R is constant in the vertical, the 0000 LT $Q_1 - Q_R$ profile would shift to the right by 1.8 K day^{-1}, essentially eliminating the upper-level cooling (i.e., no overall cooling from detraining cloud material). While the actual Q_R profile is not known, Q_R can vary significantly in the vertical in the presence of clouds, being sensitive to such factors as cloud-type distributions and their moisture content (e.g., Hartmann and Recker 1986) thus making a precise interpretation of Q_1 profiles more difficult. At 0600 LT, the low-level heating seen at 0000 LT and the upper-level heating seen at 1200 LT occur with equal frequency, which causes the average 0600 LT profile to have no discernable heating maximum.

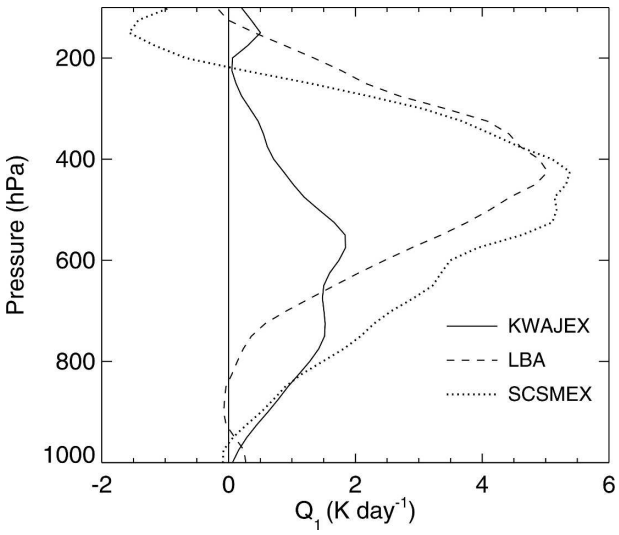

FIG. 4. Field campaign average Q_1 profiles.

[1] Vertical profiles of Q_R were not available for this study.

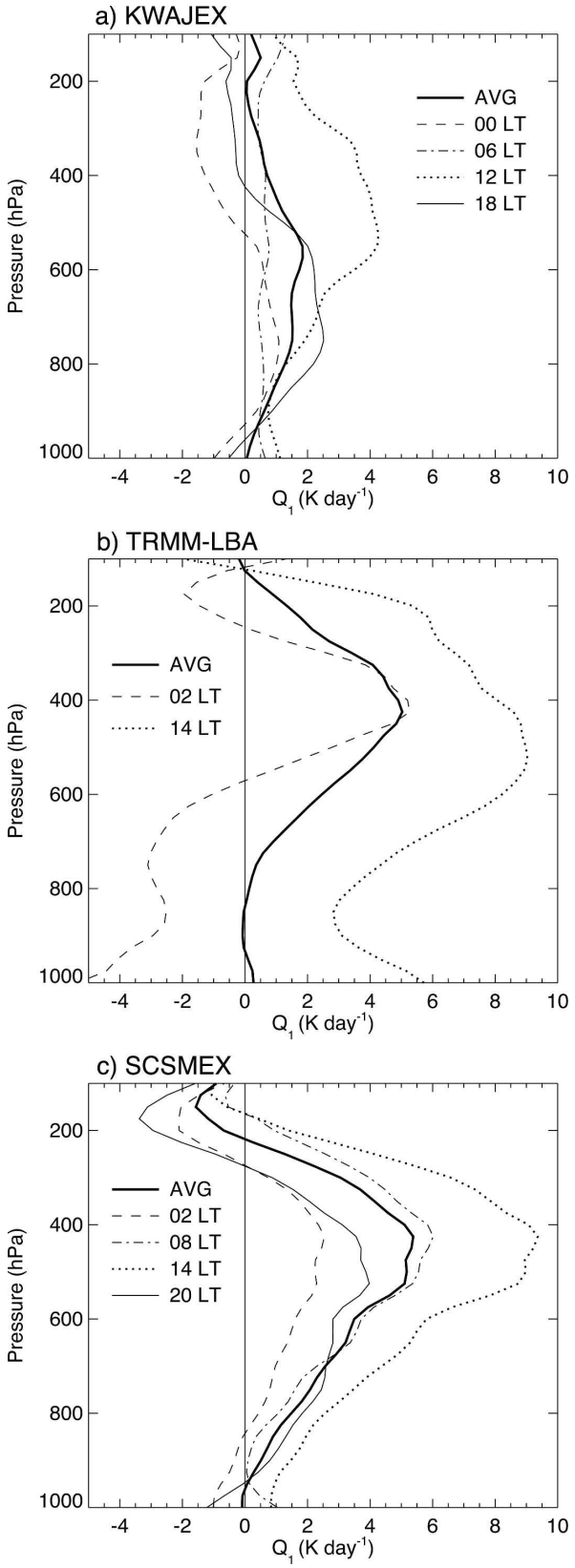

FIG. 5. Diurnal Q_1 variations for each field campaign. The thick, solid line represents each field campaign's average Q_1 profile.

Weak diurnal variations in KWAJEX Q_1 occur near the surface, with warming early in the day (0600 and 1200 LT) and cooling later in the day (1800 and 0000 LT). As the day progresses, the absorption of solar radiation by water vapor may decrease relative humidity at low levels and thus increase the evaporative cooling of falling rain, especially in the convective downdrafts associated with the 1800 and 0000 LT convection. Also, Q_1 variations at low levels (below 925 hPa) may reflect weak but discernable boundary layer diurnal effects from the small island site at which the surface fluxes were measured.

Q_1 peak magnitudes range from 4.3 K day^{-1} at 1200 LT to 1.1 K day^{-1} at 0000 LT. In contrast, the diurnal cycle of rainfall during KWAJEX was relatively small; the maximum average rain rate was 7.2 mm day^{-1} for the 6-h period centered on 1200 LT and the minimum was 5.4 mm day^{-1} for the 6-h period centered on 0000 LT (Table 1). Furthermore, the rain rate was essentially the same at 1800 LT as at 0000 LT. Thus, the large diurnal variations in the Q_1 profile suggest that other processes besides rainfall production, such as morning stratiform cloud decks, evening cumulus congestus, and diurnal variations in Q_R, are important contributors to the diurnal variability of Q_1 during KWAJEX.

Figure 5b shows a large diurnal cycle in vertical heating structure during TRMM-LBA.[2] The 1400 LT Q_1 profile has a wide maximum of 9 K day^{-1} between 600 and 400 hPa, indicating the predominance of deep convective cells. This profile occurs near the time of maximum heating of the land surface and is consistent with visual cloud observations that showed a maximum of cumulonimbus in the afternoon over the TRMM-LBA region (Strong et al. 2005). The 0200 LT profile has an upper-level maxima of 5.3 K day^{-1} at 400 hPa and significant cooling below 600 hPa, a shape very similar to the idealized stratiform latent heating profile in Fig. 1. These mean profiles are significantly different by a *t* test and are consistent with radar observations that indicate only 30%–45% of the rain is stratiform in the afternoon and early evening, whereas 60%–70% of the rain is stratiform in the morning (stratiform rain fractions are based on the radar dataset in Rickenbach et al. 2002). However, the extreme stratiform aspect of the 0200 LT profile requires further discussion.

[2] For the diurnal variational analysis, the operational soundings are most effective at constraining the Q_1 profiles between the 0000 and 1200 UTC (or 2000 and 0800 LT) launch times via the $\partial s/\partial t$ term in (1), so only the 0200 and 1400 LT profiles are shown. However, TRMM-LBA Q_1 average profiles based on wind regimes and rain thresholds presented in later sections should not be as sensitive to this temporal sampling issue.

Stratiform rain in the Tropics, as we define it, forms from aging convective cells (Houze 1997). Therefore, stratiform rain necessarily occurs in conjunction with deep convection. However, the strong low-level cooling in the 0200 LT Q_1 profile suggests that large stratiform rain areas exist separate from deep convection. Rickenbach (2004) points out that extensive mesoscale convective systems (MCSs) form near the east coast of Brazil and travel westward, often reaching the TRMM-LBA field campaign domain in the early morning hours, well after the convective peak of the system, thereby explaining at least some of the extreme stratiform character of the Q_1 profile. Rickenbach also noted the existence of nocturnal midlevel cloudiness, separate from the propagating systems. These cloud systems may not produce much rain, but could also contribute to the top heaviness of the nighttime Q_1 profile.

TRMM-LBA had a strong diurnal cycle in rainfall, with a minimum rain rate of 2.3 mm day^{-1} at 0800 LT and a maximum rain rate of 11.7 mm day^{-1} at 1400 LT (Table 1). The 0200 LT rain rate of 5.8 mm day^{-1} was also less than half of the afternoon maximum rain rate. While more rain (and thus latent heating) occurs at 1400 LT, the 0200 LT Q_1 profile provides an important contribution to the total mean profile, likely because of the large cloud coverage of the early morning mesoscale systems (see also Machado et al. 2002). At the surface, the diurnal variations in Q_1 are large because of the large variation of surface fluxes associated with diurnal temperature variations. The diurnal amplitude of the latent heat fluxes in TRMM-LBA was 5 times larger than in KWAJEX, while the peak sensible heat fluxes were an order of magnitude larger (T. O'Halloran 2004, personal communication).

SCSMEX has the largest diurnal variation in Q_1 peak magnitude and the smallest diurnal variation in the Q_1 profile shape between the three field campaigns (Fig. 5c). Each SCSMEX Q_1 profile has upper-level maxima between 400–500 hPa with smaller heating magnitudes at low levels (the near-surface diurnal variation of warming earlier in the day and cooling later in the evening is very similar to that in KWAJEX). However, the heating maximum at 400 hPa is much larger at 1400 LT than at 0200 LT—9.4 K day^{-1} versus 2.5 K day^{-1}. These two profiles are significantly different using a *t* test; however, the 1400 LT profile is not significantly different than the 0800 LT profile and is only significantly different from the 2000 LT profile above 575 mb.

Over the ocean, large MCSs often reach their greatest extent in the early morning hours (Mapes and Houze 1993; Chen and Houze 1997) so one would expect an early morning maximum in Q_1 instead of an afternoon maximum. During SCSMEX, however, satellite and ship radar data show that convective systems formed along the southern coast of China in the early morning and propagated south and east over the variational analysis domain as mature and decaying MCSs during the course of the day (Aves and Johnson 2003). This MCS cycle would explain the afternoon maximum in Q_1 and has also been observed off the north coast of Borneo (Houze et al. 1981), off the west coast of Sumatra (Mori et al. 2004), and in the Bay of Bengal (Zuidema 2003). This process is postulated to be a result of early morning coastal convection that forms from convergence of the land breeze with the prevailing low-level mean flow. These MCSs then propagate away from the coast over the adjacent oceans with speeds that suggest gravity wave dynamics are involved (Yang and Slingo 2001; Mapes et al. 2003b). SCSMEX also has a strong diurnal cycle of rainfall; average rain rates are 14.8 mm day^{-1} at 1400 LT and 8.9 mm day^{-1} at 0200 LT (Table 1). Therefore, the difference in Q_1 magnitude is related in large part to rainfall variations, although diurnal variations in $\langle Q_R \rangle$ (Table 1) should not be neglected.

5. Q_1 dependencies on the large-scale flow

While diurnal variations appear to explain a large part of the Q_1 vertical structure, each of the field campaign locations experience large-scale flow variations that also have the potential to affect the heating profile. Sobel et al. (2004) and Cetrone and Houze (2006) showed that the most organized systems over the Marshall Islands during KWAJEX occurred in association with westward-propagating synoptic-scale disturbances (although eastward-propagating Kelvin waves were also evident and may have some effect on convective organization). We composited the KWAJEX Q_1 profiles into averages centered on the easterly wave positions based on the time series of the 700-hPa meridional wind in order to show Q_1 profiles within the northerlies leading into the trough, the trough axis, the southerlies leading into the ridge axis, and the ridge of an easterly wave (as delineated in Fig. 3a). This compositing is akin to the methodology in Thompson et al. (1979, see their Fig. 2). Figure 3a indicates that 12 trough passages occurred during KWAJEX with an average period of 4.3 days. Table 2 indicates how many 6-h Q_1 profiles were used in each composite. Within the low-level northerlies (i.e., pretrough), Fig. 6a shows a bottom-heavy Q_1 profile (i.e., a primary maximum of 2.2 K day^{-1} at 800 hPa), implying that shallow convection predominates before the arrival of the trough. The Q_1 profile within

TABLE 2. Large-scale flow regime average rain rates and number of 6-h Q_1 profiles used in the average profile.

KWAJEX			TRMM-LBA			SCSMEX		
Wave position	Rain rate (mm day^{-1})	Number of 6-h Q_1 profiles	Wind regime	Rain rate (mm day^{-1})	Number of 6-h Q_1 profiles	Monsoon phase	Rain rate (mm day^{-1})	Number of 6-h Q_1 profiles
Pretrough	6.3	54	Easterly	6.1	75	Preonset	0.1	32
Trough	7.3	56	Westerly	7.1	67	Onset	16.7	32
Posttrough	8.0	61				Postonset	28.5	48
Ridge	1.4	29						

the trough shifts upward with a double maxima of ~2 K day^{-1} at 750 and 550 hPa, indicating equal contributions from shallow and deep convection. The most top-heavy heating profile occurs after the passage of the trough (the upper-level maximum is 3 K day^{-1} between 600–400 hPa), which suggests that the greatest contribution during this phase of the wave is from more organized convective systems with mature stratiform rain regions. The Q_1 profile reverses to cooling during the passage of the ridge when convection effectively ceases. The maximum cooling value approaches −2 K day^{-1} at 425 hPa. The Q_1 profiles are consistent with the rain variations within the wave (Table 2), which show the lowest rain amounts during the passage of the ridge (1.4 mm day^{-1}) and the highest rain amounts after the trough (8.0 mm day^{-1}). Reed and Recker (1971) also found the lowest precipitation values in the ridge at Kwajalein (their Fig. 11), but the rain maximum was in the trough (although significant rain occurred posttrough). The different wave position of the precipitation maximum may be due to variations in large-scale shear or wave activity from year to year. These results support previous studies concerning storm type evolution within an easterly wave (Reed and Recker 1971; Reed et al. 1977; Thompson et al. 1979) and demonstrate that waves also affect the vertical structure of Q_1 over Kwajalein.

Halverson et al. (2002), Laurent et al. (2002), and Rickenbach et al. (2002) showed that the convective systems over the western Amazon during TRMM-LBA exhibit distinct differences depending on the direction of the low-level zonal flow. The westerly regime is associated with a large anticyclone over South America that channels strong, low-level winds along the east side of the Andes that eventually turn west over the TRMM-LBA field campaign domain. The easterly regime is associated with low-level winds coming directly from the east coast of Brazil. Figure 6b composites TRMM-LBA Q_1 profiles by the easterly and westerly regime designations in Rickenbach et al. (2002); the regime designations are also shown in Fig. 3b. The shape of both Q_1 profiles is similar; the height of maximum heating is near 400 hPa and there is relatively little heating at low levels. However, the easterly regime profile has a weaker upper-level maximum (4.5 K day^{-1} versus 5.6 K day^{-1} in the westerly regime) and indicates heating at low levels rather than cooling. Precipitating systems in the easterly regime tend to be more convective and less extensive in area, such that the more stratiform and areally extensive systems that occur during the westerly regime would tend to have a stronger upper-level heating maximum and more cooling at low levels. In addition, the westerly regime had slightly higher rain accumulations than the easterly regime (7.1 mm day^{-1} versus 6.1 mm day^{-1}; Table 2), which would contribute to the larger Q_1 maximum. When the Q_1 profiles in Fig. 6b are subset to account for only moderate to heavy rain periods (not shown), there is substantially more low-level heating for both regimes and the westerly heating maximum remains near 400 hPa, while the easterly heating maximum becomes broader and shifts lower. In addition, the easterly regime has larger heating rates during strong convective events because of higher conditional rain rates (Cifelli et al. 2004). In a general sense, the profiles in Fig. 6b are consistent with the regime-dependent dual-Doppler analysis of Cifelli et al. (2004); however, discrepancies (especially at low levels) may be attributed to the different datasets and time periods considered.

Johnson and Ciesielski (2002) have already described the Q_1 variations associated with the different phases of the monsoon evolution over the South China Sea during SCSMEX using a sounding budget analysis. For consistency, we perform similar comparisons using the variational analysis method (Fig. 6c). We defined the onset and postonset active periods by matching low-level westerly wind reversals with the presence of significant precipitation. Our periods are slightly longer than Johnson and Ciesielski's 7-day definitions and are illustrated in Fig. 3c; daily rain rates and the number of 6-h Q_1 profiles used in the average for each period are shown in Table 2. Very little convection occurs before the onset of the monsoon and Fig. 6c shows that the preonset Q_1 profile is almost representative of clear-sky

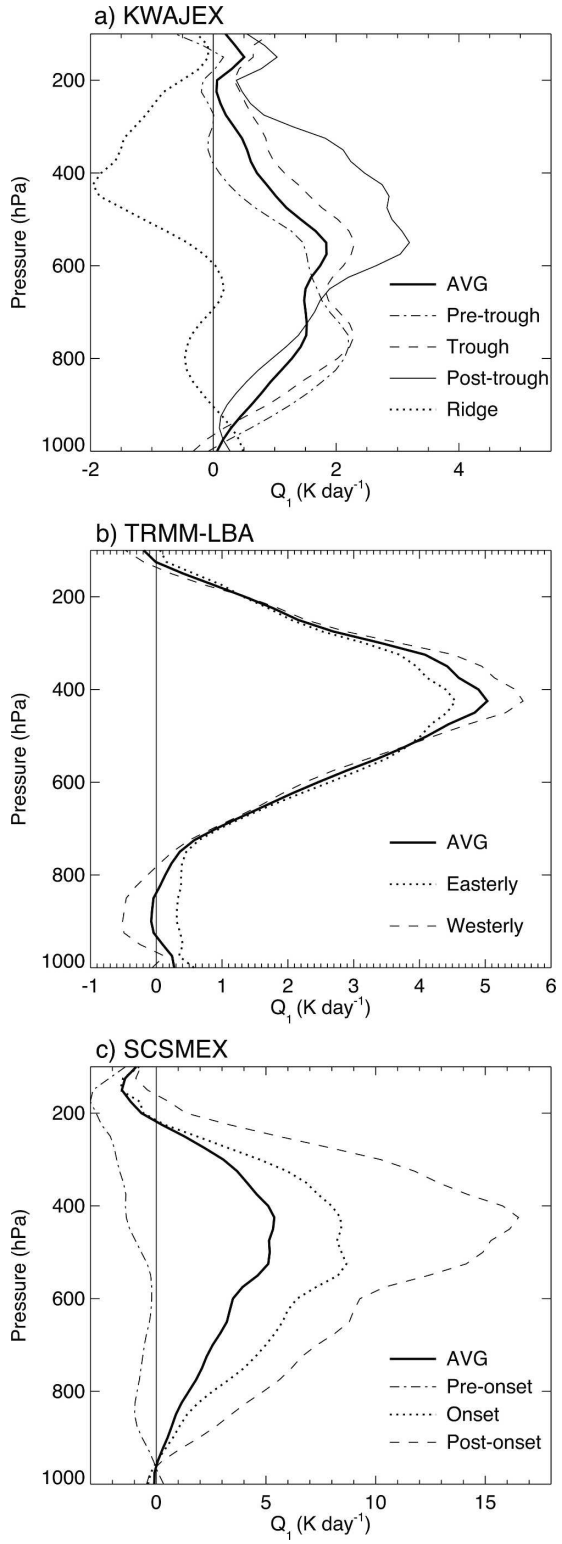

FIG. 6. Large-scale flow Q_1 variations for the (a) KWAJEX easterly wave positions, (b) TRMM-LBA easterly and westerly low-level wind regimes, and (c) SCSMEX monsoon phases. The thick, solid line represents each field campaign's average Q_1 profile.

radiative cooling values[3] of 1–2 K day^{-1}. The onset of the monsoon has a maximum in heating of ~8 K day^{-1} from 600 to 400 hPa. A radar analysis for the SCSMEX onset period (15–25 May 1998) found the stratiform rain fraction over the northern South China Sea to be 26% (Johnson et al. 2005), which is considerably less than the 40% fraction typically observed in the Tropics (Schumacher and Houze 2003a). Johnson et al. (2005) attributed this low stratiform rain fraction during the onset period to weak instability and relatively dry upper-tropospheric air, which would inhibit the development of large stratiform regions. The postonset active monsoon has generally more stratiform rain and a larger and higher maximum of heating (16.5 K day^{-1} at 400 hPa). The variational analysis profiles are in good agreement with Johnson and Ciesielski (2002) and indicate the importance of temporal variations in the Q_1 heating structure during the monsoon.

6. Rain thresholds on Q_1

This section explores variations in Q_1 based on raining and nonraining periods. Figure 7 represents the time period (7–11 August or Julian days 219–223) leading up to the largest and most organized MCS during KWAJEX. Convection was generally present all five days, but cells were scattered and unorganized for most of the period, especially before an easterly wave trough passage on Julian day 222. Figure 7a shows the radar-based precipitation time series and Fig. 7b shows the Q_1 variational analysis time series for the 5-day period. On Julian day 219, there was little rain in the variational analysis domain and weak warming (<2.5 K day^{-1}) in the lower troposphere and slightly stronger cooling (−5 K day^{-1}) in the upper troposphere. This heating signature likely resulted from shallow to moderate convection with some detrainment (cf. Fig. 1) and Q_R cooling (Table 1). Visual observations from Kwajalein also indicate numerous cumulus clouds of moderate vertical development at this time. On Julian day 220, low rain accumulations coincided with the passage of an easterly wave ridge and the subsequent suppression of convection, resulting in weak tropospheric cooling. At 0000 UTC (1200 LT) on Julian day 221, rain amounts in the variational analysis domain were beginning to increase and relatively strong heating (5 K day^{-1}) at low levels

[3] Cooling values <−2 K day^{-1} that occur above 200 hPa may be caused by excessive subsidence induced by terrain blocking effects across the Philippines during the preonset period (Johnson and Ciesielski 2002). However, the variational analysis appears to be an improvement in constraining this upper-level cooling compared to sounding-only budget analyses.

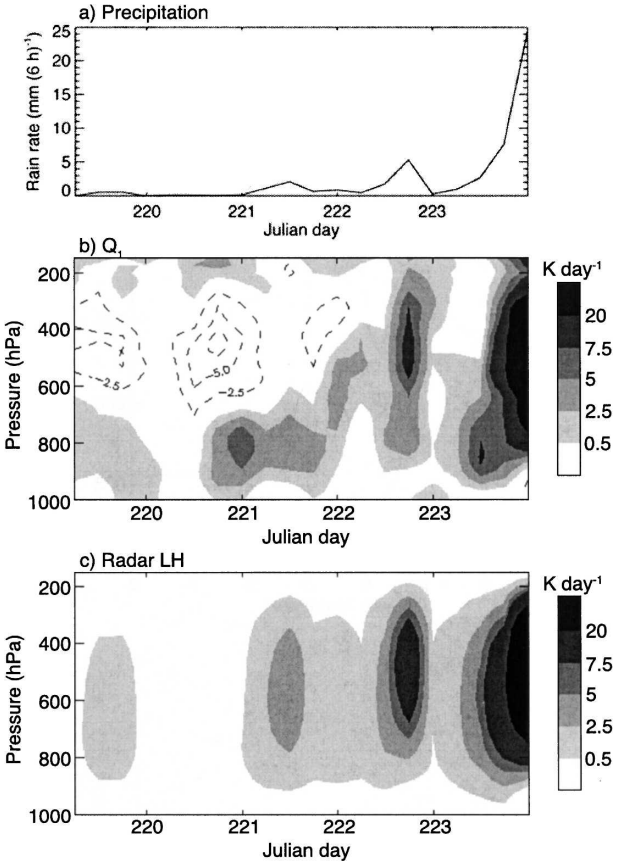

FIG. 7. KWAJEX (a) radar precipitation, (b) variational analysis Q_1, and (c) radar-derived latent heating for 7–11 Aug 1999 based on 6-h data. Dashed lines in (b) indicate cooling.

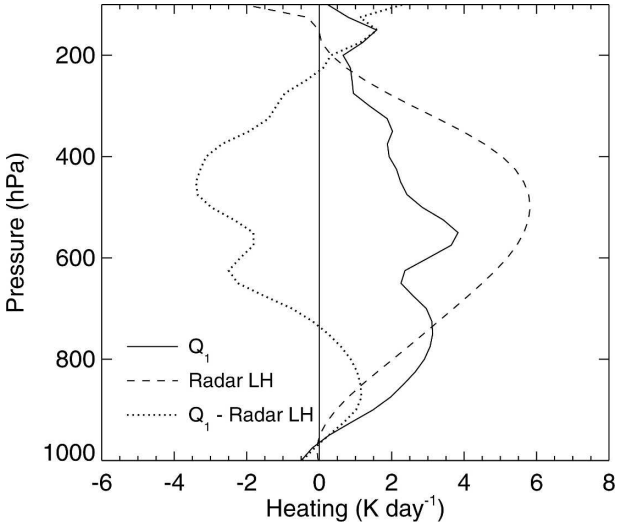

FIG. 8. Average Q_1 and radar-derived latent heating profiles for 7–11 Aug 1999. The dotted line represents the difference between Q_1 and the radar-derived latent heating.

and strong cooling (-7.5 K day^{-1}) aloft was present. At midday Q_R is near zero, so the variational analysis domain was likely populated by numerous strongly detraining cumulus congestus at this time. The cooling aloft disappeared as the rain peaked on Julian day 221, suggesting a slight increase in deep convection and/or a decrease in midlevel detrainment. After the rain peak on Julian day 221, visual observations indicated an abundance of midlevel cloud decks that may have contributed to the midlevel heating and cooling couplet around 0000 UTC on Julian day 222. An easterly wave trough passed at this time and by the end of Julian day 222, rain amounts had increased, accompanied by an increase in heating (>7.5 K day^{-1}) throughout the troposphere as the convection deepened. Enhancement in the heating profile occurs between 600 and 400 hPa, the expected peak for deep convective and stratiform rain areas. A drop in rain accumulation on Julian day 223, accompanied by a strong low-level maximum (>5 K day^{-1}) in heating, precedes the robust mesoscale system that had 6-h rain accumulations >20 mm and heating values >20 K day^{-1} throughout much of the troposphere.

Figure 7c shows the latent heating time series derived from the Kwajalein radar data. The latent heating estimation is described in Schumacher et al. (2004), but briefly, the technique distributes the column-integrated latent heating calculated from the radar-observed surface precipitation in the vertical based on a weighting of the idealized stratiform, deep convective, and shallow convective profiles in Fig. 1. Therefore, a rainy period with no stratiform or deep convective rain would simply be a scaled version of the shallow convective profile, while a rainy period with 50% stratiform rain and 50% deep convective rain would be a scaled composite of the two profiles. On Julian days 219–220, only weak heating (<1 K day^{-1}) is evident. Very little precipitation fell on those days and since the radar technique only calculates latent heating profiles when there is surface rain, the Q_1 profile variations associated with nonprecipitating clouds, as well as the Q_R component and the vertical transport of heat by eddies, are not captured. The latent heating on Julian day 221 is elevated compared to the variational analysis Q_1 time series, which could in part be due to the heights of the idealized profiles in Fig. 1 and the inability of the radar to see shallow nonprecipitating clouds. The strong elevated latent heating centers on Julian days 222 and 223 agree well with the Q_1 structures in Fig. 7b in height and magnitude, despite the idealized aspect of the latent heating calculations.

Figure 8 compares the average heating profiles from Figs. 7b,c. The average radar latent heating profile has

a larger and more elevated heating maximum and less heating at low levels than the average sounding budget Q_1 profile. The difference between the two profiles suggests the importance of shallow convection and the potential of upper-level evaporation of detrained cloud material to the overall diabatic heating profile during the 5-day period. In addition, the radar calculation does not include the net radiative cooling of the atmospheric column, which will account for some of the top-heavy cooling in the difference profile. These issues should be considered when latent and total diabatic heating estimates are made from satellites.

To differentiate each field campaign's Q_1 profiles relative to rainfall amount (and thus total latent heating), Fig. 9 separates Q_1 into heavy, moderate, and light/no-rain profiles. Table 3 denotes the criteria for each designation. Cumulative distributions of 6-h rain rates were made for each field campaign. The heavy rain category represents the profiles associated with the heaviest rain rates that in total account for 70% of the overall rainfall (but only approximately 25% of the total occurrence). The moderate rain category represents the profiles that account for the next heaviest rain rates and 25% of the total rainfall (and approximately 25% of the overall occurrence). The light/no rain category represents the rest of the cumulative rain rate distribution and accounts for about half of the total occurrence, but only 5% of the total rain amount.

The heavy rain profile during KWAJEX (Fig. 9a) has a broad maximum of 10 K day^{-1} between 550 and 450 hPa that is associated with deep convective and stratiform clouds and a lesser secondary low-level maximum ~750 hPa that is associated with shallow convective clouds. Thus, both shallow and deep convection are important for the overall rain production and vertical structure of heating at Kwajalein. The moderate rain profile is bottom heavy, again suggestive of the importance of shallow convection over the tropical Pacific. This result is consistent with the prevalence of shallow precipitating convection over the tropical oceans as observed by the TRMM Precipitation Radar (Short and Nakamura 2000; Schumacher and Houze 2003b). The light/no-rain profile shows preferential cooling (up to 2 K day^{-1}) at upper levels. Clouds during the light/no-rain periods will be mostly nonprecipitating, so the cooling aloft may reflect detrainment from shallow cumulus and cumulus congestus clouds and/or variations in the radiative cooling profile; that is, more cooling above and less cooling below the nonprecipitating clouds. The cooling aloft lowers the upper-level heating maximum in the average KWAJEX profile to 550 hPa.

The heavy rain profile during TRMM-LBA (Fig. 9b) also has a broad heating maximum (~13 K day^{-1}) be-

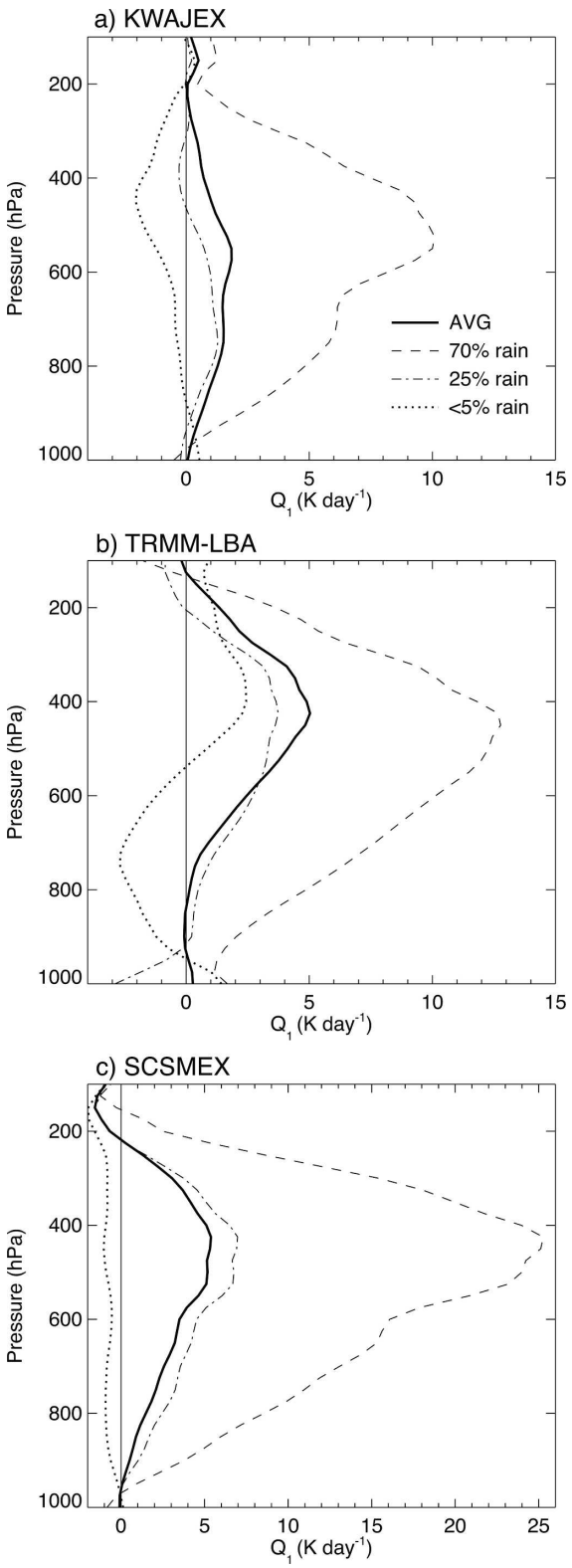

FIG. 9. Q_1 profiles for each field campaign based on thresholds of heavy (70% of rain), moderate (25% of rain), and light/no-rain (<5% of rain) rain rates. The thick, solid line represents each field campaign's average Q_1 profile.

TABLE 3. Rain-rate thresholds and percent of total occurrence for heavy (70% of total rain), moderate (25% of total rain), and light/no-rain (<5% of total rain) rain accumulations.

	KWAJEX		TRMM-LBA		SCSMEX	
Rain fraction	Rain rate (mm day^{-1})	Occurrence	Rain rate (mm day^{-1})	Occurrence	Rain rate (mm day^{-1})	Occurrence
70%	>8.4	22%	>10.5	23%	>25	18%
25%	2.0–8.4	33%	2.9–10.5	28%	6.4–25	20%
<5%	<2.0	45%	<2.9	49%	<6.4	62%

tween 550 and 450 hPa. While there is no distinct secondary low-level maximum associated with shallow convection, there is still substantial low-level heating in the heavy rain profile. In contrast, the moderate rain profile shows heating up to 3 K day^{-1} at upper levels, with no heating at lower levels. This profile is consistent with TRMM PR observations that show that shallow precipitating convection is less common over land. The light/no-rain profile shows cooling at low levels (on the order of -3 K day^{-1}) and heating up to 2 K day^{-1} above 400 hPa. This Q_1 signature likely results from the remnant stratiform cloud regions that advect or appear over the TRMM-LBA region in the early morning hours (section 4), combined with clear-sky cooling. The bottom-heavy cooling of the light/no-rain profile causes the average TRMM-LBA Q_1 profile to be top heavy.

The heavy rain profile during SCSMEX (Fig. 9c) is the most top heavy of the three field campaigns with a 25 K day^{-1} maximum at 400 hPa; however, low-level heating is still present. The moderate rain profile is also top heavy although low-level heating from shallow convection is a large contributor. Thus, the vertical heating structure over the South China Sea during the monsoon is determined largely by MCSs with significant stratiform components with some contribution from shallow convection. The light/no-rain profile most closely approximates the standard clear-sky radiative cooling profile, exhibiting values ~ -1 K day^{-1} throughout much of the troposphere.

7. Conclusions

This study has used sounding network data from three TRMM field campaigns and analyzed the data using the same methodology [i.e., Zhang and Lin's (1997) variational analysis] to compare Q_1 variations in different tropical environments. KWAJEX occurred over the open ocean; its convective events were short lived (i.e., <6 h in duration) or advected quickly over the variational analysis domain and were often associated with easterly wave activity. The average Q_1 profile during KWAJEX had two maxima and was the most bottom-heavy profile of the three field campaigns. TRMM-LBA occurred over land; its convective events were also relatively short-lived and were linked to the diurnal cycle and the large-scale flow over Bolivia and Brazil. TRMM-LBA's average Q_1 profile was the most top heavy of the three experiments. SCSMEX occurred over ocean in a monsoon regime; its convective events were long lasting with distinct active and break periods dictated by the evolution of the monsoon. The SCSMEX average Q_1 profile was also top heavy, but evidenced more low-level heating than the TRMM-LBA average profile. The SCSMEX oceanic monsoon and KWAJEX open ocean profiles are consistent with previous sounding budget comparisons by Frank and McBride (1989), who found that the Q_1 profiles over the ocean during the during the Australian monsoon had generally higher altitude of heating maxima than over the open ocean in the east Atlantic.

The diurnal cycle caused especially large Q_1 shape and peak magnitude variations at each location with afternoon and evening processes generally contributing more to the bottom-heavy aspect of the average Q_1 profiles and early and late morning processes contributing more to the top-heavy aspect (although this is not the case for SCSMEX). Over Kwajalein, shallow to moderately deep convection (with potentially significant detrainment and upper-level radiative cooling) appears to be prevalent during the afternoon and evening, while more organized precipitating systems tend to occur in the later morning hours. These modes of convection factor strongly into the low- and upper-level heating maxima in the average KWAJEX Q_1 profile, respectively. Based on previous studies over the southwestern Amazon, deep precipitating convection is observed to be common in the afternoon, while MCSs and remnant stratiform regions from convective systems originating near the Brazilian coast and more locally produced midlevel cloud systems appear to predominate in the early morning. The TRMM-LBA Q_1 diurnal profiles are consistent with these observations with both afternoon and early morning rain and cloud processes contributing to the top heaviness of the av-

erage TRMM-LBA Q_1 profile. The SCSMEX daytime Q_1 profile is top heavy as a result of convective systems forming along the China coast in the early morning hours and then propagating over the northern South China Sea during the day as mature and decaying MCSs. The MCSs appear to weaken and/or exit the variational domain in the late evening and early morning hours, thus decreasing the magnitude of the nighttime Q_1 profile significantly. The proximity of the SCSMEX variational analysis domain to land disrupts the weak diurnal signal in precipitation typically associated with tropical ocean locations.

Large-scale flow variations also affect the Q_1 profile at each location. After the passage of an easterly wave trough, the KWAJEX Q_1 profile is more top heavy than before the trough passage. This difference is consistent with the evolution of convection from shallow to moderate vertical development before a passage of a wave trough, to deeper convection during the trough passage, and to robust stratiform rain regions after the passage (e.g., Takayabu et al. 1996; Straub and Kiladis 2003). The TRMM-LBA Q_1 profile is more top heavy when westerly low-level winds predominate over western Brazil, consistent with previous studies that have shown convective systems in the westerly regime to be more areally extensive and stratiform in nature than the convective systems in the easterly regime. The SCSMEX Q_1 profile is more top heavy during the postonset active phase of the monsoon versus the onset, which is consistent with TRMM Precipitation Radar observations that show an increase in stratiform rain fraction after the monsoon begins (Schumacher and Houze 2003a).

Finally, Q_1 profiles vary significantly based on how much it is raining. During each field campaign, the heaviest rain periods (i.e., 70% of the total rain accumulation) account for about 25% of total occurrence and the bulk of the heating. In addition, the Q_1 profiles during these periods are very top heavy because of the importance of MCSs in rain production in the Tropics. Varying low-level heating occurs during the heavy rain periods depending on the convective cloud population. KWAJEX has a distinct low-level peak in Q_1 due to shallow convection (SCSMEX less so), whereas TRMM-LBA has a more continuous population of moderate to deep convection. The moderate rain periods (i.e., 25% of the total rain accumulation) also account for about 25% of the total occurrence and tend to favor lower-level Q_1 peaks, especially over the oceanic site of Kwajalein. When there is little to no rain (accounting for ~50% of total occurrence), tropospheric cooling predominates although cooling tends to be stronger at upper levels over Kwajalein and at lower levels over southwestern Brazil compared to the SCSMEX profile that approximates the radiative clear-sky cooling of the tropical atmosphere.

The above variations in Q_1 provide a challenge to models and satellite retrievals in determining the vertical structure of heating. Do models (both those used in reanalysis datasets and general circulation simulations) sufficiently capture the cloud changes associated with the diurnal cycle, shifts in large-scale flow, and rain variations? In terms of retrievals, heating estimates are very dependent on the method of measurement (Tao et al. 2006). For example, radars can only observe the precipitating portion of cloud systems so they will miss nonprecipitating features of Q_1. Infrared measurements provide cloud cover and a proxy of precipitation, but lack sufficient vertical information to calculate Q_1 profiles. The results of this study point to the importance of observing cloud systems and the large-scale environment with a multiplicity of measurement platforms to accurately describe the vertical variations in heating associated with tropical cloud systems to which the general circulation responds.

Acknowledgments. Many people and institutions contributed to gathering and processing the data used in this research. In particular, we thank Jose Fuentes for the KWAJEX and TRMM-LBA surface flux data; Sandra Yuter for her version of quality-controlled KWAJEX sounding data and for pointing out an error in the first KWAJEX rainfall analysis; Walt Peterson, Rob Cifelli, and Tom Rickenbach for the TRMM-LBA radar and gauge data; and Bill Rossow for the ISCCP data. The first author would also like to thank Bob Adler and the rest of Code 912 for their hospitality during her summer sojourn at GSFC. Useful comments on the manuscript were provided by Steve Nesbitt and an anonymous reviewer. This research was supported by NASA's Summer Faculty Fellowship Program, NSF Grant ATM-0449782 to Texas A&M University, the NASA TRMM Program and NSF to the Stony Brook University, and NASA Grant NNGO4GA22G to Colorado State University.

REFERENCES

Aves, S., and R. H. Johnson, 2003: The diurnal cycle of oceanic convection over the South China Sea during the Southeast Asian monsoon. Preprints, *10th Conf. on Mesoscale Processes,* Portland, OR, Amer. Meteor. Soc., CD-ROM, 5.4.

Betts, A. K., J. D. Fuentes, M. Garstang, and J. H. Ball, 2002: Surface diurnal cycle and boundary layer structure over Rondonia during the rainy season. *J. Geophys. Res.,* **107,** 8065, doi:10.1029/2001JD000356.

Carey, L. D., R. Cifelli, W. A. Petersen, and S. A. Rutledge, 2000: Preliminary report on TRMM-LBA rainfall estimation using

the S-Pol radar. Colorado State University, Department of Atmospheric Science Paper 697, 19 pp.

Cetrone, J., and R. A. Houze Jr., 2006: Characteristics of tropical convection over the ocean near Kwajalein. *Mon. Wea. Rev.,* **134,** 834–853.

Chan, J. C. L., W. X. Wi, and J. J. Xu, 2002: Mechanisms responsible for the maintenance of the 1998 South China Sea summer monsoon. *J. Meteor. Soc. Japan,* **80,** 1103–1113.

Chen, S. S., and R. A. Houze Jr., 1997: Diurnal variation and life-cycle of deep convective systems over the tropical Pacific warm pool. *Quart. J. Roy. Meteor. Soc.,* **122,** 689–719.

Ciesielski, P. E., and R. H. Johnson, 2006: Contrasting characteristics of convection over the northern and southern South China Sea during SCSMEX. *Mon. Wea. Rev.,* **134,** 1041–1062.

Cifelli, R., L. Carey, W. A. Petersen, and S. A. Rutledge, 2004: An ensemble study of wet season convection in southwest Amazonia: Kinematics and implications for diabatic heating. *J. Climate,* **17,** 4692–4707.

Frank, W. M., and J. L. McBride, 1989: The vertical distribution of heating in AMEX and GATE cloud clusters. *J. Atmos. Sci.,* **46,** 3464–3478.

Halverson, J. B., T. Rickenbach, B. Roy, H. Pierce, and E. Williams, 2002: Environmental characteristics of convective systems during TRMM-LBA. *Mon. Wea. Rev.,* **130,** 1493–1509.

Hartmann, D. L., and E. E. Recker, 1986: Diurnal variation of outgoing longwave radiation in the Tropics. *J. Climate Appl. Meteor.,* **25,** 800–812.

——, H. H. Hendon, and R. A. Houze Jr., 1984: Some implications of the mesoscale circulations in tropical cloud clusters for large-scale dynamics and climate. *J. Atmos. Sci.,* **41,** 113–121.

Houze, R. A., Jr., 1982: Cloud clusters and large-scale vertical motions in the Tropics. *J. Meteor. Soc. Japan,* **60,** 396–410.

——, 1989: Observed structure of mesoscale convective systems and implications for large-scale heating. *Quart. J. Roy. Meteor. Soc.,* **115,** 425–461.

——, 1997: Stratiform precipitation in regions of convection: A meteorological paradox? *Bull. Amer. Meteor. Soc.,* **78,** 2179–2196.

——, S. G. Geotis, F. D. Marks Jr., and A. K. West, 1981: Winter monsoon convection in the vicinity of North Borneo. Part I: Structure and time variation of the clouds and precipitation. *Mon. Wea. Rev.,* **109,** 1595–1614.

——, S. Brodzik, C. Schumacher, S. E. Yuter, and C. R. Williams, 2004: Uncertainties in oceanic radar rain maps at Kwajalein and implications for satellite validation. *J. Appl. Meteor.,* **43,** 1114–1132.

Johnson, R. H., 1976: The role of convective-scale precipitation downdrafts in cumulus and synoptic-scale interactions. *J. Atmos. Sci.,* **33,** 1890–1910.

——, and P. E. Ciesielski, 2002: Characteristics of the 1998 summer monsoon onset over the northern South China Sea. *J. Meteor. Soc. Japan,* **80,** 561–578.

——, T. M. Rickenbach, S. A. Rutledge, P. E. Ciesielski, and W. H. Schubert, 1999: Trimodal characteristics of tropical convection. *J. Climate,* **12,** 2397–2418.

——, S. A. Aves, P. E. Ciesielski, and T. D. Keenan, 2005: Organization of oceanic convection during the onset of the 1998 east Asian summer monsoon. *Mon. Wea. Rev.,* **133,** 131–148.

Lau, K. M., and Coauthors, 2000: A report of the field operations and early results of the South China Sea Monsoon Experiment (SCSMEX). *Bull. Amer. Meteor. Soc.,* **81,** 1261–1270.

——, X. F. Li, and H. T. Wu, 2002: Evolution of the large scale circulation, cloud structure and regional water cycle associated with the South China Sea monsoon during May-June, 1998. *J. Meteor. Soc. Japan,* **80,** 1129–1147.

Laurent, H., L. A. T. Machado, C. A. Morales, and L. Durieux, 2002: Characteristics of the Amazonian mesoscale convective systems observed from satellite and radar during the WETAMC/LBA experiment. *J. Geophys. Res.,* **107,** 8054, doi:10.1029/2001JD000337.

Lin, X., and R. H. Johnson, 1996: Heating, moistening and rainfall over the western Pacific during TOGA COARE. *J. Atmos. Sci.,* **53,** 3367–3383.

Machado, L. A. T., H. Laurent, and A. A. Lima, 2002: Diurnal march of the convection observed during TRMM-WETAMC/LBA. *J. Geophys. Res.,* **107,** 8064, doi:10.1029/2001JD000338.

Mapes, B. E., and R. A. Houze Jr., 1993: Cloud clusters and superclusters over the oceanic warm pool. *Mon. Wea. Rev.,* **121,** 1398–1415.

——, P. E. Ciesielski, and R. H. Johnson, 2003a: Sampling errors in rawinsonde-array budgets. *J. Atmos. Sci.,* **60,** 2697–2714.

——, T. T. Warner, and M. Xu, 2003b: Diurnal patterns of rainfall in northwestern South America. Part III: Diurnal gravity waves and nocturnal convection offshore. *Mon. Wea. Rev.,* **131,** 830–844.

Mori, S., and Coauthors, 2004: Diurnal land-sea rainfall peak migration over Sumatera Island, Indonesia Maritime Continent by TRMM satellite and intensive rawinsonde soundings. *Mon. Wea. Rev.,* **132,** 2021–2039.

Nesbitt, S. W., and E. J. Zipser, 2003: The diurnal cycle of rainfall and convective intensity according to three years of TRMM measurements. *J. Climate,* **16,** 1456–1475.

Nigam, S., C. Chung, and E. DeWeaver, 2000: ENSO diabatic heating in ECMWF and NCEP–NCAR reanalyses, and NCAR CCM3 simulation. *J. Climate,* **13,** 3152–3171.

Nitta, T., and S. Esbensen, 1974: Heat and moisture budget analyses using BOMEX data. *Mon. Wea. Rev.,* **102,** 17–28.

Ooyama, K., 1987: Scale-controlled objective analysis. *Mon. Wea. Rev.,* **115,** 2476–2506.

Petersen, W. A., S. W. Nesbitt, R. J. Blakeslee, R. Cifelli, P. Hein, and S. A. Rutledge, 2002: TRMM observations of intraseasonal variability in convective regimes over the Amazon. *J. Climate,* **15,** 1278–1294.

Rangno, A. L., and P. V. Hobbs, 2005: Microstructures and precipitation development in cumulus and small cumulonimbus clouds over the warm pool of the tropical Pacific Ocean. *Quart. J. Roy. Meteor. Soc.,* **131,** 639–673.

Reed, R. J., and E. E. Recker, 1971: Structure and properties of synoptic-scale wave disturbances in the equatorial western Pacific. *J. Atmos. Sci.,* **28,** 1117–1133.

——, D. C. Norquist, and E. E. Recker, 1977: The structure and properties of African wave disturbances as observed during Phase III of GATE. *Mon. Wea. Rev.,* **105,** 317–333.

Rickenbach, T. M., 2004: Nocturnal cloud systems and the diurnal variation of clouds and rainfall in southwestern Amazonia. *Mon. Wea. Rev.,* **132,** 1201–1219.

——, R. N. Ferreira, J. B. Halverson, D. L. Herdies, and M. A. F. Silva Dias, 2002: Modulation of convection in the southwestern Amazon basin by extratropical stationary fronts. *J. Geophys. Res.,* **107,** 8040, doi:10.1029/2000JD000263.

Rossow, W. B., A. W. Walker, D. Beuschel, and M. Roiter, 1996: International Satellite Cloud Climatology Project (ISSCP) description of new cloud datasets. Rep. WMO/TD 737, World Climate Research Program, World Meteorological Organization, 115 pp.

Roy, B., J. B. Halverson, and J. H. Wang, 2004: The influence of radiosonde "age" on TRMM field campaign soundings humidity correction. *J. Atmos. Oceanic Technol.,* **21,** 470–480.

Sardeshmukh, P. D., 1993: The baroclinic problem and its application to the diagnosis of atmospheric heating rates. *J. Atmos. Sci.,* **50,** 1099–1112.

Schumacher, C., and R. A. Houze Jr., 2000: Comparison of radar data from the TRMM satellite and Kwajalein oceanic validation site. *J. Appl. Meteor.,* **39,** 2151–2164.

——, and ——, 2003a: Stratiform rain in the tropics as seen by the TRMM Precipitation Radar. *J. Climate,* **16,** 1739–1756.

——, and ——, 2003b: The TRMM Precipitation Radar's view of shallow, isolated rain. *J. Appl. Meteor.,* **42,** 1519–1524.

——, ——, and I. Kraucunas, 2004: The tropical dynamical response to latent heating estimates derived from the TRMM Precipitation Radar. *J. Atmos. Sci.,* **61,** 1341–1358.

Short, D. A., and K. Nakamura, 2000: TRMM radar observations of shallow precipitation over the tropical oceans. *J. Climate,* **13,** 4107–4124.

Silva Dias, M. A. F., and Coauthors, 2002: Cloud and rain processes in a biosphere-atmosphere interaction context in the Amazon Region. *J. Geophys. Res.,* **107,** 8072, doi:10.1029/2001JD000335.

Simpson, J., R. F. Adler, and G. R. North, 1988: Proposed Tropical Rainfall Measuring Mission (TRMM) satellite. *Bull. Amer. Meteor. Soc.,* **69,** 278–295.

Sobel, A. H., S. E. Yuter, C. S. Bretherton, and G. N. Kiladis, 2004: Large-scale meteorology and deep convection during TRMM KWAJEX. *Mon. Wea. Rev.,* **132,** 422–444.

Straub, K. H., and G. N. Kiladis, 2003: The observed structure of convectively coupled Kelvin waves: Comparison with simple models of coupled wave instability. *J. Atmos. Sci.,* **60,** 1655–1668.

Strong, C., J. D. Fuentes, M. Garstang, and A. K. Betts, 2005: Daytime cycle of low-level clouds and the tropical convective boundary layer in southwestern Amazonia. *J. Appl. Meteor.,* **44,** 1607–1619.

Takayabu, Y. N., K. M. Lau, and C. H. Sui, 1996: Observation of a quasi-2-day wave during TOGA COARE. *Mon. Wea. Rev.,* **124,** 1892–1913.

Tao, W. K., J. Simpson, S. Lang, M. McCumber, R. Adler, and R. Penc, 1990: An algorithm to estimate the heating budget from vertical hydrometeor profiles. *J. Appl. Meteor.,* **29,** 1232–1244.

——, C. L. Shie, J. Simpson, S. Braun, R. H. Johnson, and P. E. Ciesielski, 2003: Convective systems over the South China Sea: Cloud-resolving model simulations. *J. Atmos. Sci.,* **60,** 2929–2956.

——, and Coauthors, 2006: Retrieval of latent heating from TRMM measurements. *Bull. Amer. Meteor. Soc.,* **87,** 1555–1572

Thompson, R. M., Jr., S. W. Payne, E. E. Recker, and R. J. Reed, 1979: Structure and properties of synoptic-scale wave disturbances in the intertropical convergence zone of the eastern Atlantic. *J. Atmos. Sci.,* **36,** 53–72.

Wang, J. J., 2004: Evolution and structure of the mesoscale convection and its environment: A case study during the early onset of the Southeast Asian summer monsoon. *Mon. Wea. Rev.,* **132,** 1104–1120.

Yanai, M., S. Esbensen, and J.-H. Chu, 1973: Determination of bulk properties of tropical cloud clusters from large-scale heat and moisture budgets. *J. Atmos. Sci.,* **30,** 611–627.

Yang, G.-Y., and J. Slingo, 2001: The diurnal cycle in the Tropics. *Mon. Wea. Rev.,* **129,** 784–801.

Yuter, S. E., R. A. Houze Jr., E. A. Smith, T. T. Wilheit, and E. Zipser, 2005: Physical characterization of tropical oceanic convection observed in KWAJEX. *J. Appl. Meteor.,* **44,** 385–415.

Zhang, M. H., and J. L. Lin, 1997: Constrained variational analysis of sounding data based on column-integrated budgets of mass, heat, moisture, and momentum: Approach and application to ARM measurements. *J. Atmos. Sci.,* **54,** 1503–1524.

——, ——, R. T. Cederwall, J. J. Yio, and S. C. Xie, 2001: Objective analysis of ARM IOP data: Method and sensitivity. *Mon. Wea. Rev.,* **129,** 295–311.

Zuidema, P., 2003: Convective clouds over the Bay of Bengal. *Mon. Wea. Rev.,* **131,** 780–798.